Rigidity percolation and geometric information in floppy origami

Siheng Chen[a] and L. Mahadevan[a,b,c,d,1]

[a]John A. Paulson School of Engineering and Applied Sciences, Harvard University, Cambridge, MA 02138; [b]Department of Physics, Harvard University, Cambridge, MA 02138; [c]Department of Organismic and Evolutionary Biology, Harvard University, Cambridge, MA 02138; and [d]Kavli Institute for Bionano Science and Technology, Harvard University, Cambridge, MA 02138

Edited by Martin van Hecke, Leiden University, Leiden, The Netherlands, and accepted by Editorial Board Member John A. Rogers March 12, 2019 (received for review December 1, 2018)

Origami structures with a large number of excess folds are capable of storing distinguishable geometric states that are energetically equivalent. As the number of excess folds is reduced, the system has fewer equivalent states and can eventually become rigid. We quantify this transition from a floppy to a rigid state as a function of the presence of folding constraints in a classic origami tessellation, Miura-ori. We show that in a fully triangulated Miura-ori that is maximally floppy, adding constraints via the elimination of diagonal folds in the quads decreases the number of degrees of freedom in the system, first linearly and then nonlinearly. In the nonlinear regime, mechanical cooperativity sets in via a redundancy in the assignment of constraints, and the degrees of freedom depend on constraint density in a scale-invariant manner. A percolation transition in the redundancy in the constraints as a function of constraint density suggests how excess folds in an origami structure can be used to store geometric information in a scale-invariant way.

origami | rigidity | percolation | information | scale-free

Origami's artistic origins harken back to the ancient art of paper folding, but it is also found in many natural settings, such as insect wings, leaves, vertebrate guts, flower petals, etc. (1–3). The beauty and complexity of these origami folding patterns arise from permutations and combinations of a few modules, of which the simplest is a unit cell with four quads and four folds intersecting at a vertex. The classic Miura-ori consists of periodic repetition of this unit cell (Fig. 1*A*). It is highly symmetric and has three important geometric properties (1). It is rigid foldable; i.e., the folding process from a flat sheet is continuous without bending any quads (2). It has only one degree of freedom (DoF) (see *SI Appendix*, section 2 for details) (3). It is also flat foldable; i.e., a flat sheet can be folded to a state where all of the planes become coplanar. These geometric properties, together with the fact that these patterns arise spontaneously from simple physical processes (2–4), have sparked much interest in the design of origami-inspired objects such as satellite sails and self-folding robots (5, 6), while also inspiring work on the mathematics and mechanics of these objects (7–11). Simultaneously, from a technological perspective, origami has become a paradigm for programming geometry (12–15). Most studies focus on origami with rigid quads (rigid-foldable origami) or elastic quads with an associated bending energy, neither of which have more than a few floppy (zero energy) degrees of freedom (16). The exceptions are the studies of configurations near the unfolded state of triangulated origami (14, 15), but the general question of the interplay between fold geometry, topology, and rigidity in origami remains open. We address this question here by studying how fold topology and geometry allow for the control of rigidity in origami structures, with the potential for storage of geometric information or making reconfigurable structural materials for use in nanotechnology, soft robotics, and architecture.

We start with a flat sheet of paper that is inextensible and unshearable, made up of quadrilateral unit cells that can all fold along their edges, and with a total of $L \times L$ quads (Fig. 1*A*) (7, 8, 17) and 4-coordinated vertices. This is the classical Miura-ori pattern that has a single zero-energy (floppy) global DoF associated with an overall rigid folding motion (5). Topologically, 4-coordinated vertices are generic in systems like crumpled paper and rigid origami (5- or higher-coordinated vertices are degenerate and will spontaneously split into two or more 4-coordinated vertices, and 3-coordinated vertices are impossible). However, generating nonperiodic folding patterns with 4-coordinated vertices is hard because of the presence of topological obstructions (13, 16). Therefore, we focus on the simple periodic Miura-ori structure, but our results should generalize to any 4-coordinated origami folded pattern which usually has a very small number of internal degrees of freedom.

To make the folded structure floppy we introduce additional folds in some of the quads by allowing them to also fold along one of their two diagonals. If the additional fold is introduced to every quad, the resulting sheet will have a large number of zero-energy DoF. A number of natural questions then pose themselves: How does the number of distinguishable geometric states in such an origami structure change as a function of the number, location, and type of excess folds or constraints? How redundant are these constraints? When and how does geometric (mechanical) cooperativity arise in the system? And how does rigidity arise in the system? Here we answer these questions and show that there is a percolation transition that heralds the onset of cooperativity in the system as a function of the density of constraints. Equivalently, we show that the number of states increases exponentially as the density of new folds increases past a critical threshold. Together these results show how we might manipulate the information storage

Significance

Origami structures are a particularly interesting class of thin-sheet–based mechanical metamaterials that rely on folds for their morphology and mechanical properties. Here, we study how excess folds in a simple origami pattern control the rigidity of the structure. Furthermore, we show that the onset of geometrical cooperativity in the system allows for information storage in a scale-free manner. Understanding how mechanical rigidity and geometric information can be simultaneously controlled in folded sheets has implications for structures on a range of scales, from graphene to architecture.

Author contributions: S.C. and L.M. designed research, conceived mathematical models, analyzed data, interpreted results, and wrote the paper. S.C. performed numerical simulations.

The authors declare no conflict of interest.

This article is a PNAS Direct Submission. M.v.H. is a guest editor invited by the Editorial Board.

[1]To whom correspondence should be addressed. Email: lmahadev@g.harvard.edu.

This article contains supporting information online at www.pnas.org/lookup/suppl/doi:10.1073/pnas.1820505116/-/DCSupplemental.

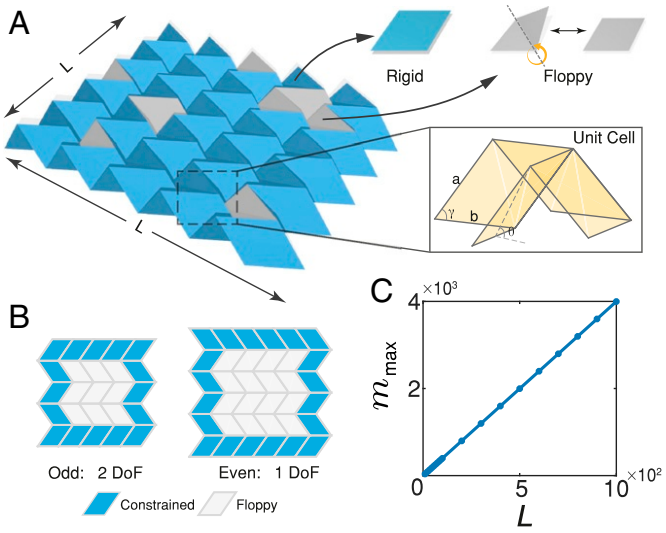

Fig. 1. Floppy origami. (*A*) Periodic Mirua-folded origami (*Left*). The unit cell has four identical parallelograms. Blue quads are rigid, and gray quads can fold about one diagonal. (*B*) If planarity constraints are enforced only on the boundary quads, the origami has one additional DoF when L is odd and no additional DoF when L is even, in addition to the global folding/expanding mode. (*C*) The line corresponds to the analytic estimate (main text) for the maximum number of DoF $m_{\max}$ as a function of L; the points correspond to results from an algebraic computation of rank of the rigidity matrix (main text).

capacity of the system by exploiting the distance to the critical threshold.

Mathematical Formulation

To calculate the (folding) degrees of freedom (m) of a sheet with a prescribed number of floppy edges that allow for out-of-plane bending, we replace the sheet by an equivalent network, where the $(L+1)^2$ vertices become nodes, the $2L(L+1)$ folds become edges, and the quad faces are replaced by additional edges along diagonal pairs of nodes. There are three types of constraints for each quad in the resulting network: (*i*) E, the four peripheral edges have constant length since the material is inextensible; (*ii*) D, one of the diagonals has constant length (to prevent any internal shear/rotation since the material is also unshearable); and (*iii*) P (quad planarity), i.e., prevention of out-of-plane folding about this internal diagonal fold, this last constraint being optional.

Constraint counting allows us to calculate the maximum DoF of the structure (18), which occurs when all of the quads are allowed to fold about the internal diagonal [we choose all of the diagonal folds along the closest pair of diagonal vertices of the quad, but the results are invariant to random choices of the diagonals (*SI Appendix*, Fig. S1)]. For a sheet with L^2 quads, there are $(L+1)^2$ vertices. When all of the quads are floppy (allowed to fold along one of the internal diagonals), there are $2L(L+1)$ type E edge constraints and L^2 type D diagonal constraints. Since each node has 3 DoF, there are at least $3(L+1)^2-(3L^2+2L)=4L+3$ degrees of freedom (m) for the network, as we have not yet imposed the quad planarity constraint. Subtracting the 6 rigid-body DoF of the system there are at least $4L-3$ degrees of freedom. We note that $m_{\max}\sim L$, suggesting that when the number of constraints exceeds kL, where k is a constant greater than 4, some of the constraints must become redundant because of the geometric dependencies imposed by piecewise isometric deformations of the sheet. As we will see later, numerical simulations confirm that the type E and type D constraints are independent and the maximum DoF ($m_{\max}$) is indeed $4L-3$ when none of the planarity constraints (type P) are enforced. If we impose all of the L^2 planarity constraints, the structure has just a single internal DoF corresponding to the rigid folding mode. What happens between these two limits?

To calculate the DoF of the system with a given number of planarity constraints, we generalize the constraint-counting argument to an infinitesimal consideration of how constraints affect the rigidity of the network defined in terms of the coordinates of all its nodes, $g(\vec{x_1},\vec{x_2},\ldots)=0$. If the coordinates of the four nodes in a quad are $\vec{x_1},\vec{x_2},\vec{x_3},\vec{x_4}$ in counterclockwise order, the quad edge-length (type E) and diagonal-length (type D) constraints can be written as

$$g=|\vec{x_i}-\vec{x_j}|^2-l^2=0 \quad [1]$$

while the planarity constraint (type P) can be written as

$$g=(\vec{x_2}-\vec{x_1})\times(\vec{x_4}-\vec{x_1})\cdot(\vec{x_3}-\vec{x_1})=0, \quad [2]$$

which is equivalent to the vanishing of the volume of the tetrahedron formed by the nodes of the quad.

If each node suffers an infinitesimal displacement defined by a vector $\vec{dx}$, the condition for infinitesimal rigidity reads

$$A\vec{dx}=0, \quad [3]$$

where the rigidity matrix A has elements $A_{ij}=\partial g_i/\partial x_j$, where $i\in[1,N]$, with N being the total number of constraints, and $j\in[1,3(L+1)^2]$ (19, 20). Each row of the matrix represents one constraint, and each column corresponds to one spatial coordinate (x, y, or z) of one of the $(L+1)^2$ nodes. Thus, the DoF of the origami system is the dimension of the null space of A. Equivalently, we can calculate the rank of A, which is the number of independent constraints, so that

$$DoF=3(L+1)^2-\mathrm{rank}(A). \quad [4]$$

Since we are interested in the internal floppy modes, we subtract the six rigid translation and rotation modes of the whole structure in reporting results of all of the following calculations. As our rigidity matrix is potentially large, but sparse, we use SuiteSparseQR for rank determination (21) (see *SI Appendix*, section 3 for more details).

Analysis

For concreteness of our calculations, we start with a periodic partially folded Miura-ori structure defined by a rhombus of side $a=b=2$, internal angle $\gamma=\pi/4$, and the dihedral angle $\theta=\arccos(\sqrt{2/3})$ [the choice of these parameters does not affect the statistical results (*SI Appendix*, Fig. S2)]. Defining c as the number of planar constraints in the floppy quads and $\rho=c/L^2$ as the density of planar constraints ($0\le\rho<1$), we randomly assign ρL^2 quads to be rigid (blue quads in Fig. 1*A*), so that the remaining $(1-\rho)L^2$ quads are floppy (gray quads in Fig. 1*A*). Eq. **4** shows that calculating $rank(A)$ is tantamount to calculating the DoF m. When $\rho=0$, the rigidity matrix A consists of $2L(L+1)$ type E constraints, L^2 type D constraints, and 0 type P constraints, as described in Eqs. **1** and **2**. Therefore, m reaches the maximum $m=m_{\max}$. Fig. 1*C* shows that $m_{\max}=4L-3$, verifying that our simple counting argument is consistent with the results of an algebraic computation.

Planarity Constraints on Boundary Quads Can Rigidify the Origami. Since $m_{\max}=4L-3$ and $m_{\min}=1$, we need at least $m_{\max}-m_{\min}=4L-4$ constraints to rigidify the system, where by rigidity we mean that the origami structure has no extra modes of motion besides the six rigid-body modes and the single internal folding mode. Since the number of boundary quads is exactly $4L-4$, we investigate the effect of constraints only

on boundary quads. Interestingly, an origami structure with planarity constraints (type P) on boundary quads is "almost" rigidified: The resulting DoF depends on whether L is odd or even (Fig. 1*B*). When L is odd, there are two DoF, i.e., one additional DoF besides the planar expanding/folding mode (*SI Appendix*, Fig. S3). When L is even, there is only one DoF corresponding to the expanding–folding mode. The difference comes from the structure of the center quads. When L is odd, there is a single center quad. In the infinitesimal mode corresponding to the extra DoF, as shown in *SI Appendix*, Fig. S3, one side of the sheet folds while the other side expands. It involves the bending of the single center quad. However, when L is even, there are four center quads, and their infinitesimal bending will in general not be mutually compatible. No matter whether L is odd or even, placing constraints on the boundary is the most efficient way to rigidify the system, since it requires only the minimum number of planarity constraints.

There are likely two reasons for how rigidification arises from planarity constraints on the boundary quads in origami. It is known that in 2D square lattices (22), if the constraint pattern satisfies the one-per-row and one-per-column condition, the whole system becomes rigid. Constraining the boundary quads in origami to be planar satisfies exactly the same condition and might thus give an intuitive explanation for our observations of how boundary-driven rigidification arises in floppy origami. Additionally, as in purely 2D systems, floppy modes in origami are more likely to involve boundary quads (22, 23); indeed, corner quads are an extreme example as they can bend without involving any quads in the bulk. Therefore, rigidifying the boundaries first might be the most efficient way to rigidify the whole system.

DoF Decreases First Linearly and Then Sublinearly As Constraint Density Increases. If we place the planarity constraints randomly on any quad in the system, we expect a certain inefficiency in their action—some will reduce the number of degrees of freedom, while others will be redundant. To understand this, we note that since there are L^2 possible locations for these constraints, while the minimal number of constraints to rigidify the origami is linear in L, generic placement of the constraints will likely lead to constraint redundancy. To quantify this further, we use an origami sheet with $L=15$ to study how the floppiness changes with the constraint density and constraint pattern (each way of spatially assigning ρL^2 type P constraints among L^2 quads is a constraint pattern). For a given ρ, we generate 200 random constraint patterns and calculate m and then sweep over $\rho \in [0, 1]$. When $\rho \ll 1$, the sparseness of constraints implies that each constraint is independent and should reduce the DoF of the system by one. At this stage, the DoF should remain independent of the constraint pattern; in Fig. 2*A*, we see that the DoF indeed

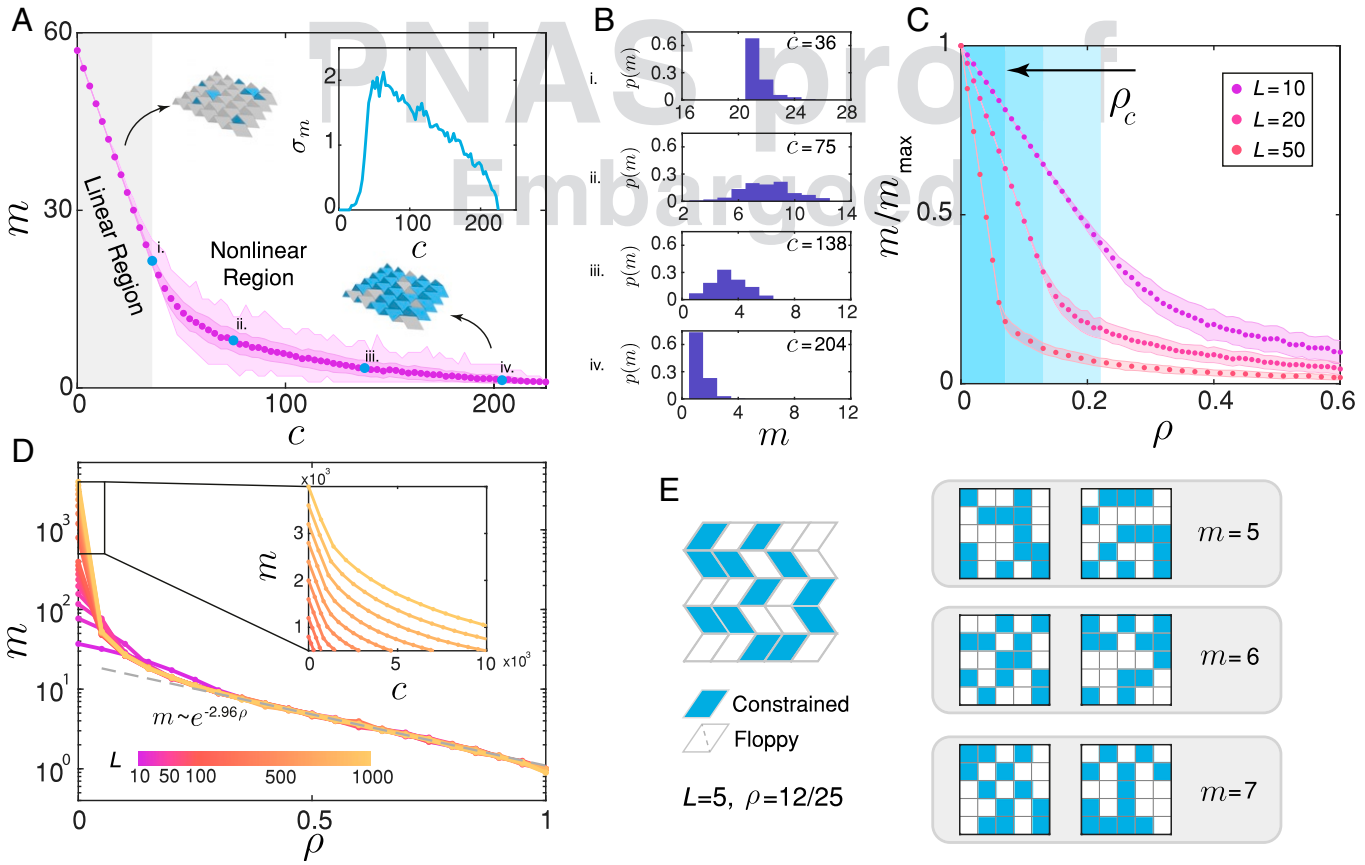

Fig. 2. DoF and geometric information in floppy origami. (*A*) DoF (m) decreases linearly first and then sublinearly as number of coplanar constraints c increases. The solid circles represent the mean of the DoF among 200 repeats, the darker shaded region shows the SD of m, and the lighter shaded region shows the range of m. (*A*, *Inset*) The variance in m starts to grow rapidly when the constraint density ρ reaches a critical value ρ_c, the onset of mechanical cooperativity. (*B*) The distribution of DoF for 200 repeats when $L=15$ for different constraint number c, in a range of different systems [indicated by blue circles in (*A*)], is skewed in the beginning and the end of the sublinear region. (*C*) The onset of mechanical cooperativity associated with sublinear decrease in m shifts leftward as system size L increases. (*D*) Simulations for different system sizes with $L \in [10, 1, 000]$ show that when $\rho \gtrsim 10\%$, the DoF in the system is essentially independent of L and decays exponentially. (*D*, *Inset*) For small ρ, DoF m decreases first linearly and then sublinearly with c. (*E*) DoF m is a function of both constraint number c and the constraint pattern; e.g., for $L=5$ and $\rho=12/25$, different constraint patterns result in different DoF (m) from 5 to 7.

decreases linearly when the constraint number density is small and increasing.

However, when the density of constraints increases sufficiently, some added constraints become redundant and thus do not reduce m. If a constraint pattern includes more redundant constraints, the corresponding DoF is larger, and vice versa. Different constraint patterns in this regime can thus lead to different m. In the neighborhood of a critical constraint density (that is to be determined), some patterns have redundant constraints while most patterns do not; in the latter case the DoF m still follows the simple rule $m = 4L - 3 - c$. Different constraint pattern realizations lead to variability in the observed number of degrees of freedom, with a leftward skewness in this limit, as expected (Fig. 2 *B*, *i*). As ρ further increases past a threshold, the mean DoF decreases sublinearly with ρ as the constraints are more likely to be redundant. Different constraint pattern realizations in this regime lead to a distribution of m that is close to being normal (Fig. 2 *B*, *ii* and *iii*). The SD (σ_m, shown in a darker shade in Fig. 2*A*) and the interquartile range Q of the distribution of m (*SI Appendix*, Fig. S4) are nonzero. We note that σ_m reaches a peak right after the transition into the nonlinear regime, and both m and σ_m decrease as ρ increases further. When $\rho \sim 1$, most of the patterns have just a single degree of freedom with $m = 1$, and only a few patterns have additional DoF. The distribution of m is skewed to the left again as expected (Fig. 2 *B*, *iv*). Finally, when $\rho = 1$, $\sigma_m = 0$ and $m = 1$.

The transition from linear to sublinear behavior in the dependence of the DoF as a function of the constraint density is similar for all system sizes L. Indeed if we rescale the DoF by its maximum (corresponding to no constraints), we see that the transition from the linear to the sublinear regime shifts to smaller ρ when L increases (Fig. 2*C*). We use the interquantile range Q of the distribution of m to define the critical transition density ρ_c corresponding to the smallest ρ when Q becomes larger than zero (*SI Appendix*, Fig. S4), a definition that is more robust than using the SD (σ_m) (see *SI Appendix*, section 5 for more information), and find that the best fit to this dependence is $\rho_c \sim L^{-1}$ (*SI Appendix*, Fig. S5). To understand this, we note that $\rho_c = c^*/L^2$, where c^* is the number of constraints at the transition. Since the redundancy must arise when $c > 4L - 3$, we expect that $c^* \sim L$, so $\rho_c \sim 1/L$. This scaling argument does not apply to systems that are small, owing to finite size effects (*SI Appendix*, Fig. S5).

In the sublinear regime, we also note that the mean DoF decreases exponentially with the density of constraints, independent of L, with $m \sim e^{-\kappa\rho}$ ($\kappa = -2.96 \pm 0.04$ when $\rho \in [0.35 - 0.80]$), as shown in Fig. 2*D*, before eventually becoming asymptotic to unity corresponding to $m = 1$. This observation suggests an alternative view of the transition between the linear and sublinear phases: If we start from the fully rigid state ($\rho = 1$) and remove the planarity constraints one at a time to make the origami sheet floppy, we will see an exponential increase in the DoF when the number of constraints is sufficiently large, although the rate at which this happens is initially much slower than the rate L^2 in the linear regime (where $m = m_{\max} - c = m_{\max} - L^2\rho$). Eventually, when $\rho \le \rho_c$, there is no cooperativity between the constraints anymore, and the exponential increase in the DoF with decreasing ρ is replaced by the linear increase. Together, these observations show that in the sublinear regime, the DoF of the origami structure shows scale-free behavior and is amenable to easy manipulation by varying the constraint density.

Additionally, we see that the range in the number of DoF m, shown in a lighter shading in Fig. 2*A*, is much larger than the variance in $m(\sigma_m)$ (shown in darker shading), which means that the different constraint patterns will lead to significantly different DoF—the extreme values of $m(\rho)$ serve as bounds on the maximum and minimum DoF possible. As a concrete example, in Fig. 2*E* we show a system with $L = 5$ and $\rho = 12/25$; i.e., 12 quads are randomly selected to be rigid while the rest can fold along their diagonals. The different constraint patterns have $m \in [5 - 7]$, depending on their geometric layout, showing how constraint density ρ and constraint pattern together determine the floppiness in the system, and thus serve as design parameters for the ability to reconfigure floppy origami to create distinguishable geometric structures that have the same number (or density) of constraints.

Information Storage in Origami. The results of the previous section suggest mechanisms for maximizing geometric information storage in origami structures as a function of the variability in $m(\rho)$. To quantify this, we first study how ρ_c and σ_m behave as a function of system size L, and we sample $L \in [10, 1,000]$ ($L = 10, 20, 30, \ldots, 100, 200, 300, \ldots, 1,000$). When ρ is smaller than ρ_c, larger origami structures have more DoF since $m_{\max} = 4L - 3$, and the DoF decreases linearly with an increase in ρ_c (Fig. 2*D*, *Inset*). Once $\rho > \rho_c$, different patterns can result in different m owing to redundancy/cooperativity, and σ_m significantly increases. [Note that the peak ρ for σ_m is slightly larger than ρ_c, but the difference is negligible for large L (*SI Appendix*, section 5).] For larger origami, the peak of σ_m occurs at smaller ρ (Fig. 3*A*), which is similar to the shift of ρ_c in Fig. 2*C*. The

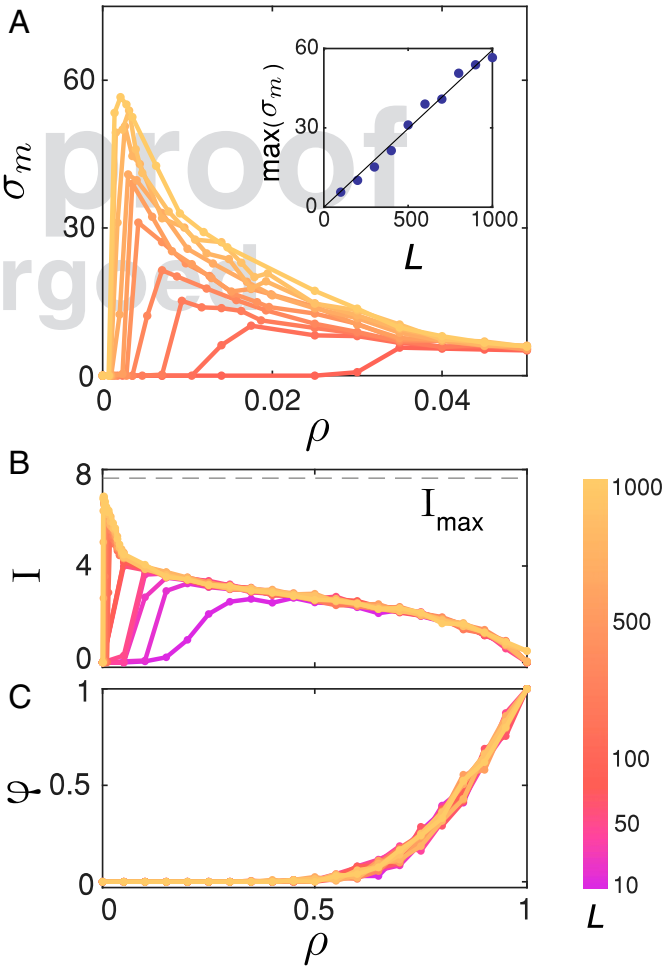

Fig. 3. Geometric information and rigidity in floppy origami. (*A*) The variance in DoF (σ_m) for *L* from 100 to 1,000. For larger *L*, the peak of σ_m occurs at smaller ρ for larger *L*, and *max*(σ_m) increases linearly with *L* (*Inset*). (*B*) The Shannon entropy *I* is maximum at ρ_c, decreases when $\rho > \rho_c$ independent of system size *L*, and characterizes the capacity for information storage in floppy origami. (*C*) The probability of being rigid (having only the single rigid-folding DoF) is completely determined by ρ, and when $\rho \ge 0.5$, this probability starts to increase and eventually saturates to unity.

peak σ_m increases almost linearly as L increases (Fig. 3*A*, *Inset*), suggesting that there is an increasing range of m associated with different constraint patterns, which results from the increasing number of constraint patterns around ρ_c [there are $\binom{L^2}{c^*}$ patterns around ρ_c and this number of combinations increases significantly with L].

In this regime, the number of floppy configurations is large, so that origami can be used to store information geometrically. Assume there are $\rho_c L^2$ rigid quads and $(1-\rho_c)L^2$ floppy quads. One can store the DoF information with the same material simply by rearranging and combining these quads to a Miura-ori structure (constructing different constraint patterns). To quantify this information capacity, we calculate the Shannon entropy of the distribution of DoF $I(\rho) = -\sum_m p(m,\rho)\log(p(m,\rho))$, where the $p(m,\rho)$ is the probability of the DoF being m among the 200 repeats for a given constraint density ρ. In Fig. 3*B*, we see that for origami with large L, the Shannon information peaks for $\rho \leq 0.05$ and decreases as ρ becomes larger. [This peak density is also slightly larger than the ρ_c we define (*SI Appendix*, section 5).] Due to the sampling limit (200 patterns per ρ), there is an upper limit in the information capacity in the system: $I = \log_2(200) = 7.64$ when there are 200 distinct DoF. We see that for large L, the maximum information capacity approaches this limit around ρ_c. When ρ is large, the information capacity is independent of L and decreases as the variance of DoF decreases.

Scale-Free Control of DoF in Origami. Strikingly, once $\rho > \rho_c$ and reaches a threshold (around 10%), the curves for different L collapse onto a single curve. Then both the DoF (Fig. 2*D*) and information capacity (Fig. 3*B*) are completely determined by the density of coplanar constraints regardless of how big the origami structure is (Fig. 2*D*), i.e., in a scale-invariant form. Furthermore, when ρ becomes sufficiently large ($\rho > 0.5$), the constraints lead to a high probability of the system being rigid (having just the rigid-folding DoF that is always present in Miura-ori), since the number of constraints required to rigidify the system $c \approx 4L - 4 \ll L^2$. Defining the probability of being rigid for a given ρ as the number of constraint patterns that leads to rigid origami divided by the number of constraint patterns possible (which we fix to be 200—the results are independent of this choice), in Fig. 3*C*, we show that this probability is a function of ρ alone. All of the results above suggest that when $\rho \gtrsim 0.1 > \rho_c$, $m = m(\rho)$ is independent of L and that the floppiness of origami is scale-free in this regime.

Percolation Behavior of Redundancy Near ρ_c. To understand the nature of the transition from the linear to sublinear decrease in DoF in the neighborhood of ρ_c, we note that the cooperativity of the constraints arises from the geometry of the folds coming together at the vertices. To quantify this, we choose a specific system of size $L = 30$, starting from a fully floppy state ($\rho = 0$), and add constraints one by one randomly. At each step, we find all of the redundant (light blue) and nonredundant (white) constraints (Fig. 4*A*), by comparing the current DoF and the DoF for a pattern with an additional planarity constraint on one of the free quads (not dark blue, which are already constrained). We iterate this process until all of the quads are constrained ($\rho = 1$) and repeat the entire process 100 times. Denoting the number of redundant and nonredundant quads as q_r and q_n, respectively, we define the "redundancy" as $r = q_r/(q_r + q_n) \in [0,1]$.

When $\rho = 0$, there are no redundant quads, i.e., $r = 0$, and each constraint reduces the DoF by one, as shown in Fig. 4*A*. When $\rho \sim \rho_c$, we see a burst of redundancy, with more redundant quads in the center than in the corners. For $\rho > \rho_c$, the number of redundant quads starts to decrease almost linearly as the number of free quads decreases (*SI Appendix*, Fig. S6), but the mean redundancy [the blue curve in Fig. 4*A*, averaged

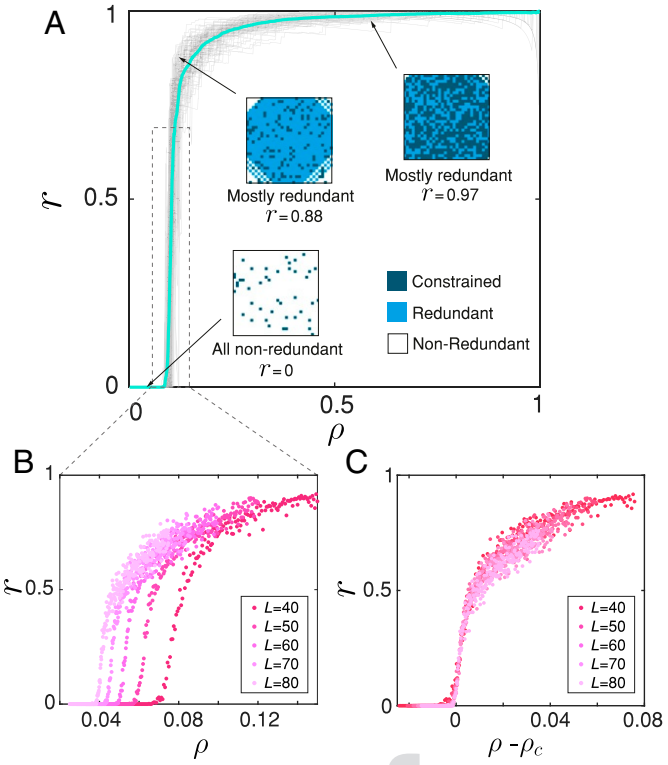

Fig. 4. Redundancy of constraints shows percolation behavior at critical density ρ_c. (*A*) Redundancy $q_r/(q_r+q_n)$ has a sharp jump around $\rho = \rho_c$ and approaches unity as ρ increases for origami with L = 30. The 100 gray lines show the change of $q_r/(q_r+q_n)$ in 100 runs, and the blue line shows the mean. Three redundancy patterns at different stages are shown (see Movie S1 for details). (*B*) The redundancy curve for different L from 40 to 80. (*C*) Redundancy percolation curves collapse after $\rho \to (\rho - \rho_c)$ (main text).

from the 100 simulations (gray lines)] keeps increasing and approaches 1. (In Movie S1, we show the process of adding constraints sequentially and the resultant change in redundancy.) To quantify the potential percolation transition in the redundancy r as a function of constraint density ρ, we explore system sizes in the range $L \in [40, 80]$, in the scale-free regime. Instead of adding constraints singly, we generate 100 random constraint patterns at a given ρ and calculate the average redundancy. In Fig. 4*B*, we see a signature of percolation at different constraint density as a function of L, with $r \to 1$ when $\rho > \rho_c$. Using finite size scaling analysis to study the percolation transition, we adopt the ansatz $r = L^{-\nu} f((\rho - \rho_c(L))L^{\xi})$ to examine the transition. We find that the redundancy curves collapse by shifting the density by $\rho_c(L)$ with $(\nu = 0, \xi = 0)$ (Fig. 4*C*) (see *SI Appendix*, Figs. S7 and S8 for more details); indeed, redundancy percolation happens at exactly the same time as Q deviates from zero. Redundancy not only increases sharply near ρ_c, but also has high variance at a given ρ around ρ_c (gray lines do not overlap in the nonlinear region in Fig. 4*A*), which means that randomly generated constraint patterns may contain a significantly different number of redundant quads. The difference in the number of redundant quads leads to different DoF and thus nonzero Q. All of the quantities m, Q, and $I(m,\rho)$ have a critical transition at $\rho = \rho_c$. We may note that this percolation transition in DoF with respect to constraint density has some similarities to rigidity percolation in 2D and 3D random networks (24, 25), but note that our problem is rather different due to the nature of the geometric embedding problem associated with having a 2D sheet bent into the third dimension. As discussed in *Mathematical Formulation*, the planarity constraint (type P) in the flat quads of Miura-ori is fundamentally different from the diagonal edge-length constraint (type D).

The former prevents volume change while the latter prevents length/area change. If we generalize our geometry of Miura-ori to more general folding patterns, with some quads bent along the diagonal, these two types of constraints will be equivalent, and we might recover the results of rigidity percolation in 3D random networks as discussed in ref. 25. See *SI Appendix*, section 2 for more details.

Discussion

The geometric complexity associated with origami has long been an artist's playground. But this ancient art form is in equal measure a rich source of mathematics and an inspiration for technology. Here, we have focused on the role of excess folds, or complexity (Latin cognate: *com* + *plicare* = fold together), in determining how excess folds can influence the rigidity of these structures. Beginning with a minimally complex geometric origami pattern associated with Miura-ori that has just a single folding degree of freedom, we have investigated how adding extra diagonal folds allows us to ask and answer questions about its potential for reconfigurability and ability to store geometric information.

When we start with a maximally floppy Miura-ori structure that is fully triangulated and introduce coplanarity constraints, the mean DoF initially decreases linearly until the constraint density $\rho = \rho_c$, beyond which the DoF starts to decrease sublinearly as geometric cooperativity sets in the sheet. This is coincident with a percolation transition in the redundancy/cooperativity in the origami structure, reminiscent of similar transitions in simple planar or 3D systems (24, 25). Simultaneously, the redundancy of coplanar constraints increases abruptly, leading to a maximum in the Shannon entropy and a maximum in the information storage capacity. This transition bears qualitative similarities to the phase transition seen in Hopfield networks that have an exponential increase in the number of memories as the connectivity crosses a critical threshold (26) and to a recent reprisal of this idea in a material model of self-assembly (27).

The presence of a percolation transition points toward some intriguing applications that include (*i*) a framework for multibit mechanical information storage, going beyond a recent 1-bit origami-based storage device (28); (*ii*) strategies for the optimal control of the number of DoF in a floppy origami structure in the neighborhood of the transition as well as deep in the scale-free regime; and (*iii*) an exploration of mechanical cooperativity in origami, similar to that in 2D networks (29, 30). Given that these chimeric denizens can move between two and three dimensions, there is clearly a lot that still remains to be explored.

ACKNOWLEDGMENTS. We thank Levi Dudte for discussions of the project during its early stages and Chris Rycroft for advice on algorithms. We also acknowledge NSF Grant DMR 14-20570 MRSEC, NSF Grant DMR 15-33985 Biomatter, and NSF Grant EFRI 18-30901 for partial financial support.

1. Kobayashi H, Kresling B, Vincent JF (1998) The geometry of unfolding tree leaves. *Proc R Soc Lond B Biol Sci* 265:147–154.
2. Bowden N, Brittain S, Evans AG, Hutchinson JW, Whitesides GM (1998) Spontaneous formation of ordered structures in thin films of metals supported on an elastomeric polymer. *Nature* 393:146.
3. Mahadevan L, Rica S (2005) Self-organized origami. *Science* 307:1740.
4. Rizzieri R, Mahadevan L, Vaziri A, Donald A (2006) Superficial wrinkles in stretched, drying gelatin films. *Langmuir* 22:3622–3626.
5. Miura K (1985) Method of packaging and deployment of large membranes in space. *Inst Space Astronaut Sci Rep* 618:1–9.
6. Felton S, Tolley M, Demaine E, Rus D, Wood R (2014) A method for building self-folding machines. *Science* 345:644–646.
7. Wei ZY, Guo ZV, Dudte L, Liang HY, Mahadevan L (2013) Geometric mechanics of periodic pleated origami. *Phys Rev Lett* 110:215501.
8. Schenk M, Guest SD (2013) Geometry of Miura-folded metamaterials. *Proc Natl Acad Sci USA* 110:3276–3281.
9. Waitukaitis S, Menaut R, Chen BGg, van Hecke M (2015) Origami multistability: From single vertices to metasheets. *Phys Rev Lett* 114:055503.
10. Silverberg JL, et al. (2015) Origami structures with a critical transition to bistability arising from hidden degrees of freedom. *Nat Mater* 14:389–393.
11. Bertoldi K, Vitelli V, Christensen J, van Hecke M (2017) Flexible mechanical metamaterials. *Nat Rev Mater* 2:17066.
12. Hawkes E, et al. (2010) Programmable matter by folding. *Proc Natl Acad Sci USA* 107:12441–12445.
13. Dudte LH, Vouga E, Tachi T, Mahadevan L (2016) Programming curvature using origami tessellations. *Nat Mater* 15:583.
14. Stern M, Pinson MB, Murugan A (2017) The complexity of folding self-folding origami. *Phys Rev X* 7:041070.
15. Chen BGg, Santangelo CD (2018) Branches of triangulated origami near the unfolded state. *Phys Rev X* 8:011034.
16. Tachi T (2009) Generalization of rigid-foldable quadrilateral-mesh origami. *J Int Assoc Shell Spatial Struct* 50:173–179.
17. Kawasaki T (1989) On the relation between mountain-creases and valley-creases of a flat origami. *Proceedings of the First International Meeting of Origami Science and Technology* ed Huzita H (Commune di Ferra and Centro Origami Duffusion, Ferrara, Italy), pp 229–237.
18. Maxwell JC (1864) L. on the calculation of the equilibrium and stiffness of frames. *Philos Mag* 27:294–299.
19. Guest S (2006) The stiffness of prestressed frameworks: A unifying approach. *Int J Solids Struct* 43:842–854.
20. Lubensky T, Kane C, Mao X, Souslov A, Sun K (2015) Phonons and elasticity in critically coordinated lattices. *Rep Prog Phys* 78:073901.
21. Davis TA (2011) Algorithm 915, SuiteSparseQR: Multifrontal multithreaded rank-revealing sparse QR factorization. *ACM Trans Math Softw* 38:8.1–8.22.
22. Ellenbroek WG, Mao X (2011) Rigidity percolation on the square lattice. *Europhys Lett* 96:54002.
23. Zhang L, Rocklin DZ, Chen BGg, Mao X (2015) Rigidity percolation by next-nearest-neighbor bonds on generic and regular isostatic lattices. *Phys Rev E* 91:032124.
24. Jacobs D, Thorpe M (1996) Generic rigidity percolation in two dimensions. *Phys Rev E* 53:3682.
25. Chubynsky M, Thorpe MF (2007) Algorithms for three-dimensional rigidity analysis and a first-order percolation transition. *Phys Rev E* 76:041135.
26. Hopfield JJ (1982) Neural networks and physical systems with emergent collective computational abilities. *Proc Natl Acad Sci USA* 79:2554–2558.
27. Murugan A, Zeravcic Z, Brenner MP, Leibler S (2015) Multifarious assembly mixtures: Systems allowing retrieval of diverse stored structures. *Proc Natl Acad Sci USA* 112:54–59.
28. Treml B, Gillman A, Buskohl P, Vaia R (2018) Origami mechanologic. *Proc Natl Acad Sci USA* 115:6916–6921.
29. Rocks JW, et al. (2017) Designing allostery-inspired response in mechanical networks. *Proc Natl Acad Sci USA* 114:2520–2525.
30. Yan L, Ravasio R, Brito C, Wyart M (2017) Architecture and coevolution of allosteric materials. *Proc Natl Acad Sci USA* 114:2526–2531.